CONF-9705118--1

SAND97-0189C

SAND--97-0189C

# Recent Advances in Mid-Infrared (3-6 micron) Emitters

R. M. Biefeld, A. A. Allerman, and S. R. Kurtz
Sandia National Laboratory, Albuquerque, NM 87185-0601

## Abstract

We describe the metal-organic chemical vapor deposition (MOCVD) of InAsSb/InAs multiple quantum well (MQW) and InAsSb/InAsP strained-layer superlattice (SLS) active regions for use in mid-infrared emitters. We have made gain-guided, injection lasers using undoped, p-type $AlAs_{0.16}Sb_{0.84}$ for optical confinement and both strained InAsSb/InAs MQW and InAsSb/InAsP SLS active regions. The lasers and LEDs utilize the semi-metal properties of a p-GaAsSb/n-InAs heterojunction as a source for electrons injected into active regions. A multiple-stage LED utilizing this semi-metal injection scheme is reported. Gain-guided, injected lasers with a strained InAsSb/InAs MQW active region operated up to 210 K in pulsed mode with an emission wavelength of 3.8-3.9 μm and a characteristic temperature of 29-40 K. We also present results for both optically pumped and injection lasers with InAsSb/InAsP SLS active regions. The maximum operating temperature of an optically pumped 3.7 μm SLS laser was 240 K. An SLS LED emitted at 4.0 μm with 80 μW of power at 300 K.

Keywords: InAsSb, Mid-infrared laser, Metal-organic chemical vapor deposition,infrared LEDs, antimonide materials.

## Introduction

Chemical sensor and infrared countermeasure technologies would become viable with the availability of high power, mid-infrared (3-6 μm) lasers and LEDs operating near room temperature. However, the performance of both type I and II Sb-based III - V mid-infrared emitters has been limited by nonradiative recombination processes (usually Auger recombination), which overwhelm radiative recombination in narrow bandgap semiconductors. Potentially, Auger recombination can be suppressed in band-structure engineered, strained InAsSb heterostructures. In this paper, we present recent advances in the metal-organic chemical vapor deposition (MOCVD) and the development of InAsSb-based, mid-infrared devices. Previously, we demonstrated an electrically injected, 3.5 μm laser with a strained and nominally dislocation free, active region.[1] The active region consisted of 10, biaxially compressed quantum wells of $InAs_{0.94}Sb_{0.06}$. InPSb cladding layers were used for optical confinement. To improve the operating characteristics of our lasers we are developing the synthesis of Al(As)Sb by MOCVD as confinement layers and InAsSb/InAsP strained-layer superlattice active regions for these devices. Along with the material development effort, we are exploring novel multi-stage (or cascaded) active regions to improve the performance of mid-infrared lasers and LEDs.

In order to reduce Auger recombination in mid-infrared (3-6 μm) lasers, several narrow bandgap III-V, strained-layer superlattices (SLSs) have been explored using MOCVD and molecular beam epitaxy (MBE) [1-11]. In both type I and type II SLS laser active regions, holes are confined to compressively strained layers, producing a low in-plane, effective mass ($|3/2,\pm3/2\rangle$) hole ground state. In compressively strained InAsSb SLSs, it is necessary to maximize the light-heavy ($|3/2,\pm1/2\rangle$ - $|3/2,\pm3/2\rangle$) hole splitting to suppress Auger recombination. For example, we have investigated the electronic properties of the InGaAs/InAsSb SLSs, and we find that the light-heavy hole splitting (≈ 30 meV) is insufficient to achieve maximum suppression of Auger recombination [1,12,13]. InAsSb SLSs incorporating barrier layers with larger valence band offsets are

required to maximize the light-heavy hole splitting through quantum confinement. Towards this goal, MBE-grown InAsSb/InAlAs and InAsSb/InAlAsSb SLS lasers have been examined with encouraging results [2,8]. In this work, we report the properties of the first InAsSb/InAsP SLS materials and devices. The InAsSb/InAsP SLS is an MOCVD variant of the most promising type I, strained InAsSb heterostructures for Auger suppression. Also, a miscibility gap, reported for InAlAsSb quaternaries, has not been found for InAsP [8]. Incorporating InAsP as a barrier layer in the active region will introduce a larger valence band offset than either of the offsets between InAs or InGaAs and InAsSb . Compared with other compressively strained InAsSb devices, initial tests on InAsSb/InAsP SLS lasers and LEDs show state-of-the-art performance. We report on the synthesis of these materials by MOCVD and their use in improved 3-6 μm, mid-infrared optoelectronic heterojunction emitters.

The injection devices described in this work contain a GaAsSb (p) / InAs (n) heterojunction to form an internal, semi-metal layer. In our devices, the semi-metal acts as an internal electron source which can eliminate many of the problems associated with electron injection in these devices, and this novel device is compatible with MOCVD materials and background doping. Furthermore, the use of an internal electron-hole source enables us to consider alternative laser and LED designs that would not be feasible with conventional, bipolar devices. Using the semi-metal, InAsSb-based multi-staged active regions can be constructed (see Figure 1) where in the absence of non-radiative losses, several photons would be generated for every carrier injected at the device contacts. A two stage LED is described in this work to demonstrate the feasibility of our idea [10]. Similar to the multi-staged InAsSb devices, the multi-staged, unipolar quantum cascade laser has received much acclaim [14], and we have reported cascaded, type II InAs/GaInSb LEDs and lasers [15,16]. The nonradiative (optical phonon) lifetimes of the unipolar devices are orders of magnitude shorter than the Auger-limited lifetimes for interband devices, and with

multi-staging, mid-infrared interband antimonide-based lasers should have lower threshold currents than unipolar quantum cascade lasers.

## Experimental

This work was carried out in a previously described MOCVD system [17,18]. We used EDMAA, TESb, and 100% arsine ($AsH_3$) as the sources for Al, Sb and As respectively, for the growth of $AlAs_xSb_{1-x}$ cladding layers. Triethylgallium (TEGa), arsine and TESb were used to grow a 400 to 2500Å GaAsSb cap on all samples to keep the $AlAs_xSb_{1-x}$ layer from oxidizing. Hydrogen was used as the carrier gas at a total flow of 8 slpm. The AlAsSb composition was determined by double crystal x-ray diffraction. Layer thickness was determined using a groove technique and was cross checked by cross sectional SEM. These thickness measuring techniques usually agreed within a few percent.

The InAsSb/InAs strained, multiple quantum wells (MQWs) and strained balanced InAsSb/InAsP SLSs were also grown by MOCVD on n-type InAs substrates. The SLSs were lattice matched to InAs with $\Delta a/a < 0.0004$. The MQWs and SLSs were grown at 500 °C, and 200 torr in a horizontal quartz reactor using trimethylindium (TMIn); TESb, 10 % $AsH_3$ in hydrogen, 100 % $PH_3$ and hydrogen as the carrier gas. A V/III ratio for the InAsSb layer of 16 to 32 with an $AsH_3/(AsH_3+TESb)$ ratio of 0.63 to 0.81 and a growth rate of 2.5 Å/second were used in the MQWs. The InAsSb layers in the SLSs were grown using a V/III ratio of 15 to 21 and an $AsH_3/(AsH_3+TESb)$ ratio of 0.59 to 0.71 at a growth rate of 2.5 Å/second. The InAsP layers were grown using a V/III ratio of 217 and an $AsH_3/(AsH_3+PH_3)$ ratio of 0.02 with an identical growth rate of 2.5 Å/second. A 15 second purge, with reactants switched out of the chamber, was used between each layer for both the MQWs and the SLSs. The MQW and SLS composition and strain were determined by double crystal x-ray diffraction.

Infrared photoluminescence (PL) was measured on all samples from 14 K up to 300 K using a double-modulation, Fourier-transform infrared (FTIR) technique which

provides high sensitivity, reduces sample heating, and eliminates the blackbody background from infrared emission spectra. Injection devices (both LEDs and lasers) also were characterized with double modulation FTIR.

## Results And Discussion

### Growth and Characterization Of InAsSb/InAs Multiple Quantum Wells

The variation of InAsSb composition with $AsH_3/(AsH_3+TESb)$ ratio for the As rich end of the $InAs_{1-X}Sb_X$ ternary are similar to those described previously for the Sb rich end of the ternary [17,18]. The composition, X, of the $InAs_{1-x}Sb_x$ quantum wells could be varied between X = 0.1 and 0.2 by changing the $AsH_3/(AsH_3+TESb)$ ratio between 0.81 and 0.63 using these growth conditions. The composition changes can be explained by the use of a thermodynamic model as previously discussed [17,18]. The model predicts that the thermodynamically more stable III/V compound will control the composition. For the InAsSb system when III/V < 1, As is preferentially incorporated into the solid and the solid-vapor distribution coefficient of Sb ($k_{Sb}$) is < 1. InAs has a lower free energy of formation, than InSb at 475-525 °C (i.e. InAs is more stable than InSb). For III/V ratios close to one, $k_{Sb}$ approaches one and for III/V ≥ 1, $k_{Sb}$ = 1. When III/V ≥ 1, all of the group V materials, including As and Sb, will be incorporated into the solid at their vapor concentrations. These trends are also found in our data for As rich InAsSb.

The high structural quality of the MQW structure is demonstrated by the narrow peaks and the large number (7) of diffraction satellites observed by double crystal x-ray diffraction. As a further indication of material quality, the photoluminescence of the MQWs could be observed at room temperature, and MQW photoluminescence was narrow with linewidths of 7-12 meV at 14 K, depending on the underlying cladding material and

pump intensity. For a change of Sb composition from x = 0.11 to 0.20 the PL peak changes from 4.0 to 6.0 μm (see Figure 2).

### Growth and Characterization of InAsP/InAsSb SLSs

The crystal quality of the SLSs was excellent with 3 to 4 orders of x-ray diffraction satellite peaks typically observed. The Sb composition could be varied between 0.13 to 0.2 while maintaining constant layer thickness for both the InAsSb and InAsP layers. For a change of Sb composition from x = 0.13 to 0.20 the PL peak changes from 3.5 to 4.4 μm while holding the layer thicknesses constant (see Figure 2). The difference in the peak wavelengths for the MQW and SLS structures for the same Sb composition is due to increased quantum confinement with the InAsP barriers. The PL wavelength could be varied from 3.2 to 3.8 μm for a change in thickness from 45 to 108 Å. For layers thicker than approximately 90 Å the x-ray diffraction patterns broadened indicating the presence of dislocations.

The band alignments and quantum confinement states for a representative InAsSb/InAsP SLS active region are shown in Figure 3. The energy levels for this $InAs_{0.88}Sb_{0.12}$ / $InAs_{0.76}P_{0.24}$ (80 Å / 80 Å) SLS were determined using a transfer matrix, 8x8 k•p calculation. Based on previous measurements of our ordered and phase separated, MOCVD-grown, InAsSb alloys, the estimated bandgap of the unstrained $InAs_{0.88}Sb_{0.12}$ alloy was 259 meV [12,19,20]. SLS valence band offsets vary linearly with composition from unstrained InAs/InSb and InAs/InP valence band offset values, 0.39 eV and -0.56 eV respectively [12,20,21]. When used as the active region, the SLS in Figure 3 will emit at 349 meV (3.6 μm) at low temperature. We estimate that the SLS has a light-heavy hole splitting of 69 meV, and emitters incorporating these SLSs should display improved performance over earlier devices with MOCVD-grown active regions. Limited by critical

layer thickness, longer wavelength InAsSb/InAsP SLSs with higher Sb and P content will display even larger light-heavy hole splittings.

## Semi-Metal Injection Laser With Pseudomorphic InAsSb Multiple Quantum Well Active Region

The band alignments for the single stage, semi-metal injection laser are shown in Figure 4. As confirmed by x-ray measurements, both the claddings and active region of the laser are commensurate with the substrate. Following a $GaAs_{0.09}Sb_{0.91}$ buffer, a 2.5 μm thick $AlAs_{0.16}Sb_{0.84}$ cladding is grown on an n-type, InAs substrate. A 200 Å, $GaAs_{0.09}Sb_{0.91}$ layer lies between the bottom cladding and a 0.6 μm thick InAs active region containing 10, pseudomorphic $InAs_{0.88}Sb_{0.12}$ quantum wells, each 90 Å thick. A 2.5 μm thick $AlAs_{0.16}Sb_{0.84}$ cladding followed by a 1200 Å, $GaAs_{0.09}Sb_{0.91}$ contact and oxidation barrier layer is grown on top of the active region. AlAsSb and GaAsSb alloys have p-type background doping levels of $10^{17}$ /cm$^3$, estimated from Hall measurements [4]. The background doping of the InAs/InAsSb active region is n-type, $10^{15}$-$10^{16}$ /cm$^3$. None of the layers in the laser structure were intentionally doped. The semi-metal nature of the p-GaAsSb / n-InAs interface is used to inject electrons into the active region.

For a wide range of Fermi energies, the GaAsSb (p) / InAs (n) heterojunction is a semi-metal, acting as a source/sink for electron-hole pairs. In forward bias (as shown in Figure 4), electrons are generated in the semi-metal and swept into the active region to recombine with holes being injected from the anode (+). Holes that recombine in the active region are replenished by holes generated in the semi-metal and swept away from the active region. Only hole transport is observed in the AlAsSb claddings (labeled points A and B in Figure 4), and over this segment, the device can be described as unipolar.

Gain-guided, stripe lasers were fabricated with Ti (50 Å) / Au (4000 Å) metallizations. The facets were uncoated. Under pulsed operation, lasing was observed in forward bias with 40x1000 or 80x1000 μm stripes. No emission occurred under reverse bias. Devices were tested with 100 nsec pulse widths at 10 kHz (0.1 % duty-cycle). Several longitudinal modes were observed in the 3.8-3.9 μm range for 80 K and 200 K operation. Characteristic of the pseudomorphic InAsSb lasers, laser emission was blue-shifted by 20 meV from the peak of the InAsSb quantum well PL, and consistent with the selection rule for the compressively strained InAsSb quantum well electron ($|1/2,\pm1/2\rangle$) - hole ($|3/2,\pm3/2\rangle$) transition, laser emission was 100% TE polarized. The lasers displayed sharp threshold current characteristics, and lasing was observed through 210 K. (Figure 5(a)) Under pulsed operation, peak power levels of 1 mW/facet could be obtained. A characteristic temperature ($T_0$) in the 30-40 K range was observed (Figure 5(b)), with the lower value (30 K) being misleading due to degradation of the device at the higher temperatures.

The use of an internal electron- hole source enables us to design multi-stage lasers and LEDs. To our knowledge, the only comparable devices are tandem solar cells where tunnel junctions are used to internally generate electrons and holes between stages. As a demonstration, we have grown a 2-stage/ 2-color LED using InAsSb quantum wells with 11% and 13% Sb in each stage [10]. Each stage is the segment A-B in Figure 4. A 600Å thick $AlAs_xSb_{1-x}$ electron barrier is placed between the 2 stages. Low temperature emission spectra from a 2-stage LED and a 1-stage LED (grown during the same run and removed from the growth chamber in the middle of the run) showed two peaks, corresponding to emission from each stage for the 2-stage device. (see Figure 6) The relative intensities of the peaks of the 2-stage device are comparable to those observed in PL, also shown in Figure 6, which indicates that electrons are independently generated in each stage.

**InAsSb/InAsP SLS Active Region Optically Pumped and Injection Lasers and LEDs**

An LED was constructed with a 0.7 μm thick, n-type, $InAs_{0.88}Sb_{0.12}$ /$InAs_{0.75}P_{0.25}$ ( 80 Å / 82 Å) SLS active region. Like the MQW devices, a semi-metal layer consisting of a 500 Å thick GaInSb (p-type) and a 500 Å thick InAs (n-type) heterojunction provided electrical injection for the LED. A 1 $mm^2$ piece of the wafer was mounted onto a header with a parabolic collector. The top contact of the LED was a 0.02" diameter Ti/Au dot. A 300K emission spectrum for the LED is shown in Figure 7(a). The large emission peak at 4 μm originates from the SLS active region; electron-hole recombination in the InAs layer produces the small peak at 360 meV. The InAsSb/InAsP SLS LED is the brightest 4 μm, room temperature device that we have produced with MOCVD. Operating the device at 1 kHz, 50% duty cycle, 200 mA average current, the average output power of the LED was 80 μW at 300 K. At 80 K the output power of the LED was 24x that observed at 300 K. The output power of our SLS device (300 K) was 5-6x that measured with the same current for LPE-grown, InAsSb alloy LEDs, obtained commercially [22].

To avoid loss mechanisms associated with electrical injection and to observe lasing with minimum heating, InAsSb/InAsP SLS lasers were characterized using low duty-cycle optical pumping. An optically pumped laser was grown on an InAs substrate with a 2.5 μm thick $AlAs_{0.16}Sb_{0.84}$ lower cladding. On top of the cladding, the active region was a 1.0 μm thick, $InAs_{0.89}Sb_{0.11}$ /$InAs_{0.77}P_{0.23}$ ( 83 Å / 87 Å) SLS. For the limited number of devices studied, neither a top cladding nor a semi-metal injection layer seemed to significantly affect laser performance under optical pumping. The SLS laser was pumped with a Q-switched Nd:YAG (1.06 μm, 20 Hz, 10 nsec pulse, focused to a 200 μm wide line), and emission was detected with an FTIR operated in a step-scan mode. Due to the

low rep-rate of the pump, approximately a 4 hour scan was required to obtain an interferogram with resolution $\geq 2$ cm$^{-1}$.

Laser emission was observed from cleaved bars, 1000 μm wide, with uncoated facets. A lasing threshold and spectrally narrowed, laser emission was seen from 80 K through 240 K, the maximum temperature where lasing occurred. (See Figure7(b) and 8(a)) As shown in Figure 7(b), the PL linewidth is ≈ 25 meV at 80K, but above threshold, the laser emission, narrowed to 3-5 meV depending on the sample, is superimposed on the broad spontaneous emission. The laser emission linewidth is limited by inhomogenieties in the material and the presence of multiple, unresolved longitudinal modes; similar behavior was observed in optically pumped type II, GaInSb/InAs lasers [7,9]. The wavelength of our laser shifts from 3.57 μm to 3.85 μm due to the decrease in bandgap over the 80-240K temperature range. At 80 K, peak powers >100 mW could be obtained. In Figure 7(b), laser emission was 6 meV higher in energy than the PL peak; for other InAsSb/InAsP SLS lasers tested, laser emission was at the PL peak energy. Generally, InAsSb/InAsP SLS laser emission occurred nearer to peak of the PL emission than previously reported for MOCVD-grown devices with pseudomorphic InAsSb MQW active regions. The temperature dependence of the SLS laser threshold is described by a characteristic temperature, $T_0 = 33$ K, over the entire range. (See Figure 8(b))

In several areas, the InAsSb/InAsP SLS laser approached performance records for III-V, bipolar lasers of comparable wavelength. We report the lowest threshold power, highest characteristic temperature, and highest operating temperature for InAsSb lasers at ≈ 3.9 μm, obtained either with pulsed injection or pulsed optical pumping [2,10,23-26]. Recently, Malin et al. reported record-setting performance for a type II, 4 μm GaInSb/InAs SLS laser pumped with a pulsed Ho:YAG laser (2.06 μm, 10 Hz) [9]. The characteristic temperature of our InAsSb/InAsP SLS device is comparable to that reported for the type II device ($T_o$= 35 K) [9]. The maximum operating temperature (270K) and threshold power ( $P_{th}$= 100 kW/ cm$^2$ @ 240K) of the type II device are marginally improved over our laser,

and unpublished results for the optically pumped, type II lasers report even further improvement [25]. However, excitation with the Ho:YAG will produce less heating and may explain much of the improvement [26]. InAsSb/InAsP, InAsSb/InAlAs, or GaInSb/InAs SLS active regions should suppress Auger recombination, and initial results for these lasers have been promising. However, ≈ 4 μm lasers with these active regions have not yet demonstrated characteristic temperatures larger than ≈ 40 K.[2,9,10,25]

We have recently demonstrated InAsSb/InAsP SLS injection lasers at 3.4 μm and 180 K. Under pulsed operation, peak power levels of 100 mW/facet (average power of 0.5 mW/facet) could be obtained at 80 K. A characteristic temperature ($T_0$) of 39 K was observed. We speculate that injection and transport of carriers in the SLS is presently limiting the performance of these devices.

## Conclusions

The growth of high quality $AlAs_xSb_{1-x}$ by MOCVD has been demonstrated and used for optical confinement layers in a 3.8-3.9 μm injection laser with a novel GaSb/InAs semi-metal electron injector. The InAsSb/InAs MQW laser operated under pulsed conditions up to 210K with a $T_o$ of 30-40K. We have also reported a 2-color LED to demonstrate multi-stage operation of semi-metal injection devices.

We have evaluated InAsSb/InAsP SLSs as active regions for MOCVD-grown, mid-infrared lasers and LEDs. Band structure calculations for these SLSs indicate that large light-heavy hole splittings (≥ 70 meV) can be achieved to suppress Auger recombination. X-ray and optical characterization of the SLSs indicate very high crystalline quality for the MOCVD-grown material and electronic properties consistent with our model of the SLS. Excellent performance was observed for an SLS LED and an optically pumped SLS laser. The semi-metal injected, broadband LED emitted at 4 μm with 80 μW of power at 300K, 200 mA average current. The optically pumped laser displayed 3.86 μm emission at 240 K, the maximum operating temperature of the laser, and a characteristic temperature of 33 K. InAsSb/InAsP SLS laser operating temperature, characteristic temperature, and

threshold power values are state-of-the-art for InAsSb lasers at ≈ 4 μm. Also, an injection InAsSb/InAsP laser was demonstrated. With nominal improvements in materials and processing and the further development of multi-stage active regions, MOCVD-grown InAsSb devices should be able to satisfy the system requirements for use in chemical sensor and infrared countermeasure technologies in the near future.

## Acknowledgments

We thank J. A.Bur and J. H. Burkhart for technical support. Our work was supported by the U.S. Dept. of Energy under contract No. DE-AC04-94AL85000. Sandia is a multiprogram laboratory operated by Sandia Corporation, a Lockheed Martin Company, for the United States Department of Energy.

## References


[1] S. R. Kurtz, R. M. Biefeld, A. A. Allerman, A. J. Howard, M. H. Crawford, and M. W. Pelczynski, "A pseudomorphic InAsSb multiple quantum well injection laser emitting at 3.5 μm," Appl. Phys. Lett. 68, pp. 1332-1334, 1996.

[2] H. K. Choi and G. W. Turner, "InAsSb/InAlAsSb strained quantum-well diode lasers emitting at 3.9 μm," Appl. Phys. Lett. 67, pp. 332-334, 1995.

[3] Y-H. Zhang, "Continuous wave operation of InAs/InAsSb midinfrared lasers," Appl. Phys. Lett., Appl. Phys. Lett. 66, pp. 118-120, 1995.

[4] R. M. Biefeld, A. A. Allerman, and M. W. Pelczynski, "The growth of n- and p-type Al(As)Sb by metal-organic chemical vapor deposition," Appl. Phys. Lett. 68, pp. 932-934, 1996.

[5] S. R. Kurtz, R. M. Biefeld, L. R. Dawson, K. C. Baucom, and A. J. Howard, "Midwave (4μm) infrared lasers and light-emitting diodes," Appl. Phys. Lett. 64, pp. 812-814, 1994.

[6] D. Z. Garbuzov, R.U Martinelli, R.J. Menna, P.K. York. H. Lee, S. Y. Narayan, and J. C. Connolly, Appl. Phys. Lett. "2.7 μm InGaAsSb/AlGaAsSb laser diodes with continuous-wave operation up to -39 °C," 67, pp. 1346-1348, 1995.

[7] D.H. Chow, R.H. Miles, T.C. Hasenberg, A.R. Kost, Y.-H. Zhang, H.L. Dunlap and L. West, "Mid-wave infrared diode lasers based on GaInSb/InAs and InAsAlSb superlattices," Appl. Phys. Lett. 67, pp. 3700-3702, 1995.

[8] H. K. Choi, G. W. Turner, M. J. Manfra, and M. K. Connors, "175 K continuous wave operation of InAsSb/InAlAsSb quantum-well diode lasers emitting at 3.5 μm," Appl. Phys. Lett. 68, pp. 2936-2338, 1996.

[9] J. I. Malin, J. R. Meyer, C. L. Felix, J. R. Lindle, L. Goldberg, C. A. Hoffman, F. J. Bartoli, C. H. Lin, P. C. Chang, S. J. Murry, R. Q. Yang, and S. S. Pei, "Type II mid-infrared quantum well lasers," Appl Phys. Lett. 68, pp. 2976-2978, 1996.

[10] A. A. Allerman, R. M. Biefeld, and S. R.Kurtz, "InAsSb-based mid-infrared lasers (3.8-3.9 μm) and light-emitting diodes with AlAsSb claddings and semi-metal electron injection grown by metal-organic chemical vapor deposition," Appl. Phys. Lett. **69**, pp. 465-467, 1996.

[11] R. J. Menna, D. Garbuznov, R. U. Martinelli, and G. H. Olsen (to be published).

[12] S. R. Kurtz, R. M. Biefeld, and A. J. Howard, "A magneto-optical determination of light-heavy hole splittings in As-rich InAsSb alloys and superlattices," Appl. Phys. Lett. **67**, pp. 3331-3333, 1995.

[13] H. P. Hjalmarson and S. R. Kurtz, Appl. Phys. Lett. "Electron auger processes in mid-infrared InAsSb/InGaAs heterostructrures," **69**, pp. 949-951, 1996.

[14] J. Faist, F. Capasso, C. Sirtori, D. L. Sivco, J. N. Baillargeon, A. L. Hutchinson, S. N. G. Chung, and A. Y. Cho, Appl. Phys. Lett., "High power mid-infrared ($\lambda \approx 5\mu m$) quantum cascade lasers operating above room temperature," **68**, pp. 3680-3682, 1996, and references therein.

[15] R. Q. Yang, C.-H. Lin, P. C. Chang, S. J. Murry, D. Zhang, S. S. Pei, S. R. Kurtz, A.-N. Chu, and F. Ren, Elect. Lett. "Mid-IR interband cascade electroluminescence in type-II quyantum wells," **32**, pp. 1621-1622 (1996).

[16] C.-H. Lin, R. Q. Yang, D. Zhang, S. J. Murry, S. S. Pei, A. A. Allerman, and S. R. Kurtz, "Quantum cascade light emitting diodes gased on type-II quantum wells," Elect. Lett. (submitted for publication) 1997.

[17] R. M. Biefeld, K. C. Baucom, and S. R. Kurtz, "The growth of $InAs_{1-x}Sb_x$/InAs strained-layer superlattices by metal-organic chemical vapor deposition," J. Crystal Growth, **137**, pp. 231-234, 1994.

[18] R. M. Biefeld, "The preparation of InSb and InAsSb by metalorganic chemical vapor deposition," J. Crystal Growth, **75**, pp. 255-263, 1986.

[19] D. M. Follstaedt, R. M. Biefeld, S. R. Kurtz, and K. C. Baucom, "Microstructures of $InAs_{1-x}Sb_x$ (x=0.07-0.14) alloys and strained-

layer superlattices," J. Electronic Materials, 24, pp. 819-825, 1995.

[20] S. R. Kurtz and R. M. Biefeld, "Magnetophotoluminescence of biaxially compressed InAsSb quantum wells," Appl. Phys. Lett. 66, pp. 364-366, 1995.

[21] Chris G. Van de Walle, Phys. Rev. B 39, 1871 (1989).

[22] Our device was compared with a 4.2 μm LED obtained from RMC Ltd., Moscow, Russia.

[23] Y. B Li, D. J. Bain, L. Hart, M. Livingstone, C. M. Ciesla, M. J. Pullin, P. J. P. Tang, W. T. Yuen, I. Galbraith, C. C. Phillips, C. R. Pidgeon, R. A. Stradling, "Band alignments and offsets is In(AsSb)/InAs superlattices," Phys. Rev. B 55, pp. 4589-4595 , 1997.

[24] H. K. Choi, G. W. Turner, and H. Q. Le, "GaSb-based semiconductor lasers in the 4-μm band," Inst. Phys. Conf. Ser. 144, pp. 1-7, 1995.

[25] C. L. Felix, J. R. Meyer, I Vurgaftman, C. H. Lin, S. J. Murry, D. Zhang, and S. S. Pei, "High-temperature 4.5 μm type II quantum well laser with Auger suppression," Photon. Tech. Lett. (in press).

[26] H. Q. Le, G. W.Turner, J. R. Ochoa, and A. Sanchez, "High-efficiency, high-temperature mid-infrared ($\lambda$ => 4mm) InAsSb/GaSb lasers" Elect. Lett. 30, pp. 1944-1945, 1994.

## Figure Captions

Figure 1. An InAsSb multi-stage laser and LED active region with semi-metal electron injection at each stage.

Figure 2. Low temperature PL ( < 20K) from 10 period 90Å $InSb_xAs_{1-x}$ / 450Å InAs MQW's and 40 period 75Å $InSb_xAs_{1-x}$ / 84Å $InAs_{.76}P_{.24}$ SLS's grown on InAs for different Sb content in the InAsSb layer.

Figure 3. Band alignments and quantum confinement state energies (drawn to scale) for an $InAs_{0.88}Sb_{0.12}$ / $InAs_{0.76}P_{0.24}$ (80 Å / 80 Å) SLS.

Figure 4. Heterojunction band alignments for the MOCVD-grown, GaAsSb/InAs semi-metal injection laser with a pseudomorphic InAsSb MQW active region. Forward bias polarity is indicated in the figure.

Figure 5. (a) InAsSb/InAs MQW semi-metal injection laser emission intensity versus peak current for various temperatures. (b) Pulsed threshold current density versus temperature. The stripe dimensions were 40x1000 μm.

Figure 6. High-resolution, 14 K LED emission spectra of a two-stage and a one-stage device incorporating semi-metal, injector active regions. Also shown is the PL spectrum for the two-stage device. The $CO_2$ feature is absent from these spectra due to nitrogen purging of the experiment.

Figure 7. (a) Emission spectrum for an LED with an $InAs_{0.88}Sb_{0.12}$/$InAs_{0.75}P_{0.25}$ ( 80 Å / 82 Å) SLS active region. The spectrum is distorted by $CO_2$ absorption lines at 290 meV. (b) Lasing and PL spectra for a laser with an $InAs_{0.89}Sb_{0.11}$/$InAs_{0.77}P_{0.23}$ ( 83 Å / 87 Å) SLS active region.

Figure 8. (a) Pulsed laser emission intensity versus optical pump power for various temperatures for an $InAs_{0.89}Sb_{0.11}$/$InAs_{0.77}P_{0.23}$ ( 83 Å / 87 Å) SLS active region. (b) Threshold optical pump power versus temperature.

Multi-stage, Strained InAsSb Active Region -

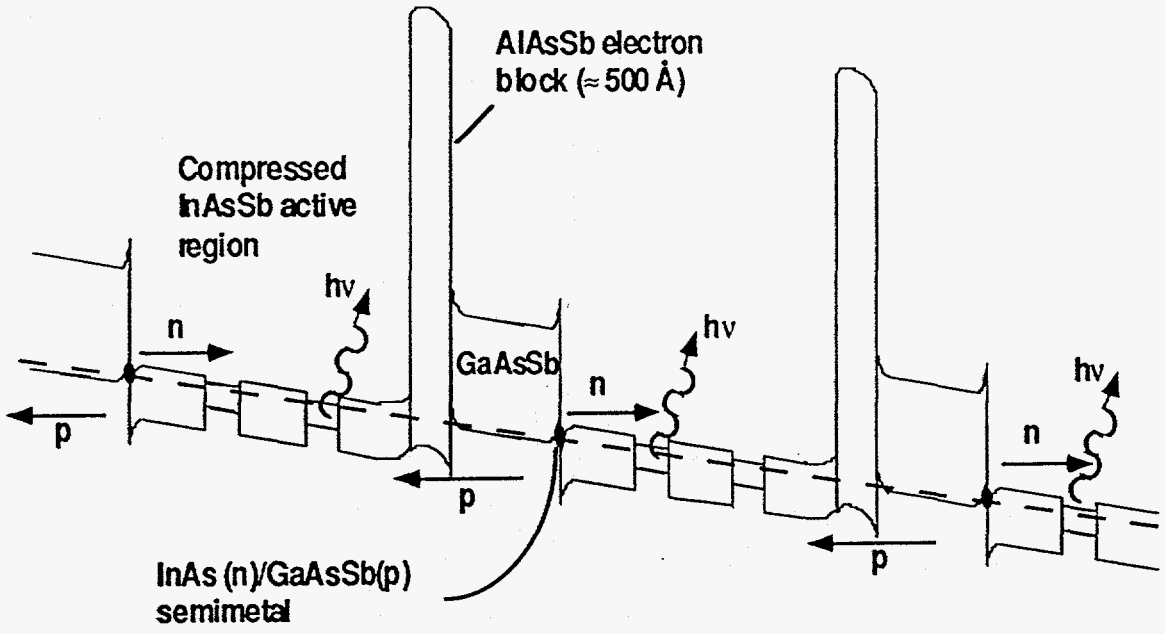


Figure 1.

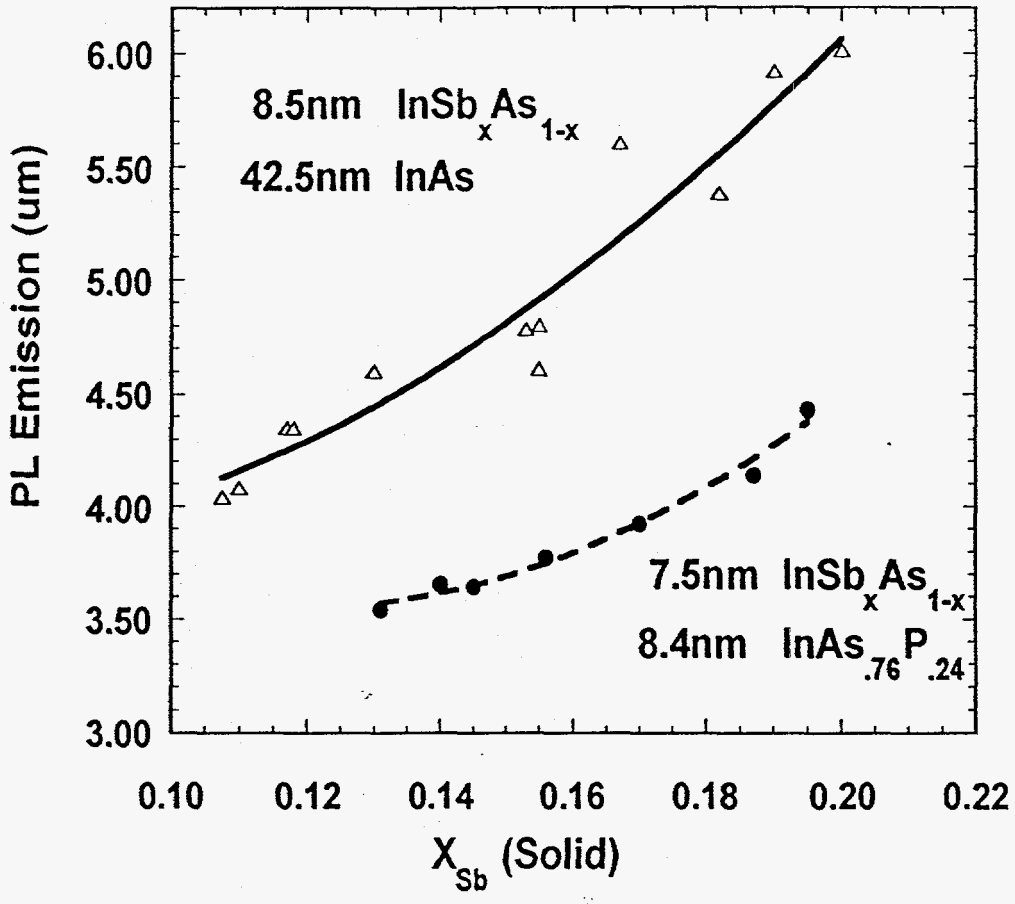
6.00
5.50
5.00
4.50
4.00
3.50
3.00
PL Emission (um)
8.5nm InSb$_x$As$_{1-x}$
42.5nm InAs
7.5nm InSb$_x$As$_{1-x}$
8.4nm InAs$_{.76}$P$_{.24}$
0.10
0.12
0.14
0.16
0.18
0.20
0.22
X$_{Sb}$ (Solid)

Figure 2.

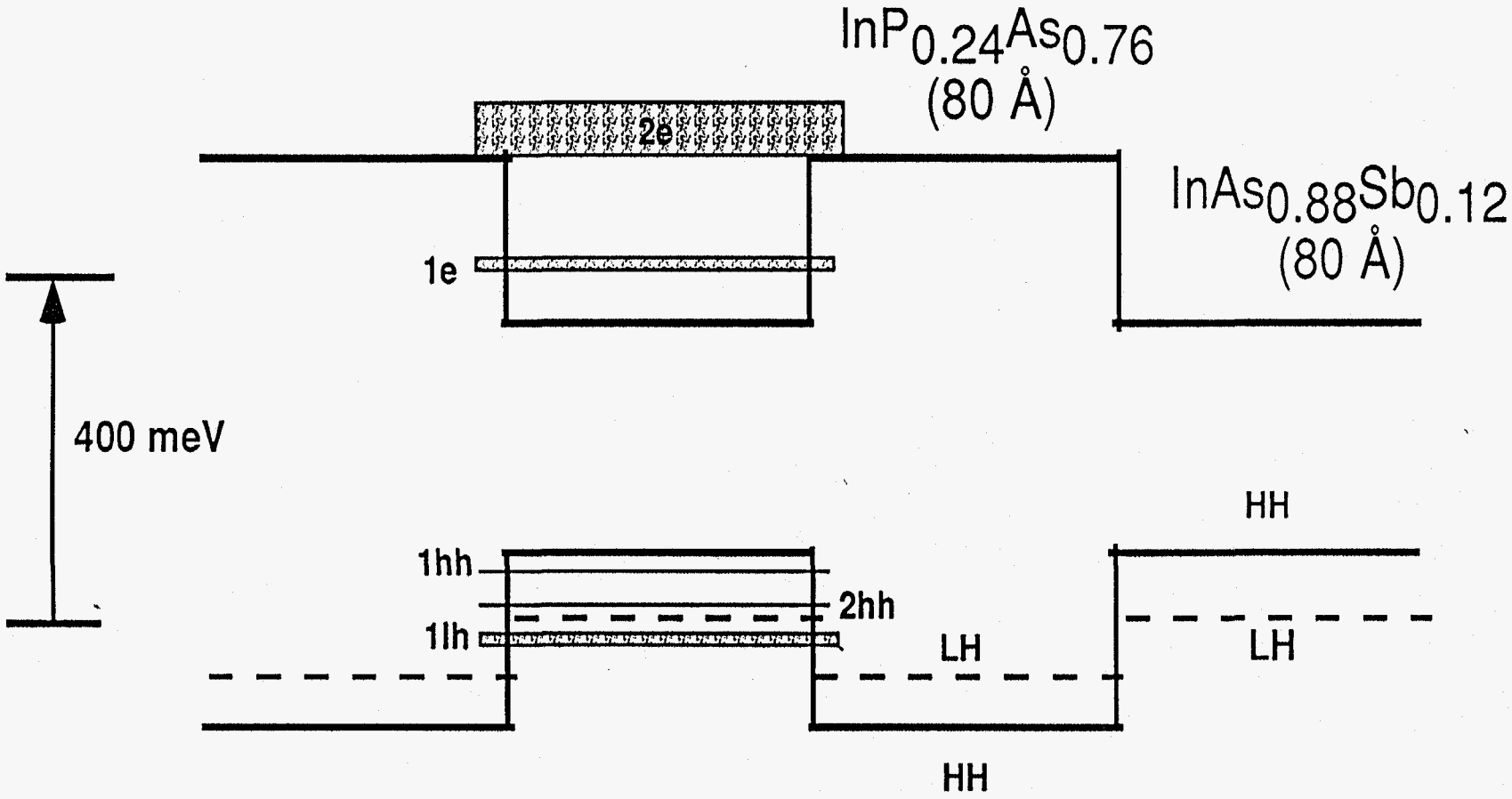
InP0.24As0.76
(80 Å)
2e
InAs0.88Sb0.12
(80 Å)
1e
400 meV
HH
1hh
2hh
1lh
LH
LH
HH

Figure 3.

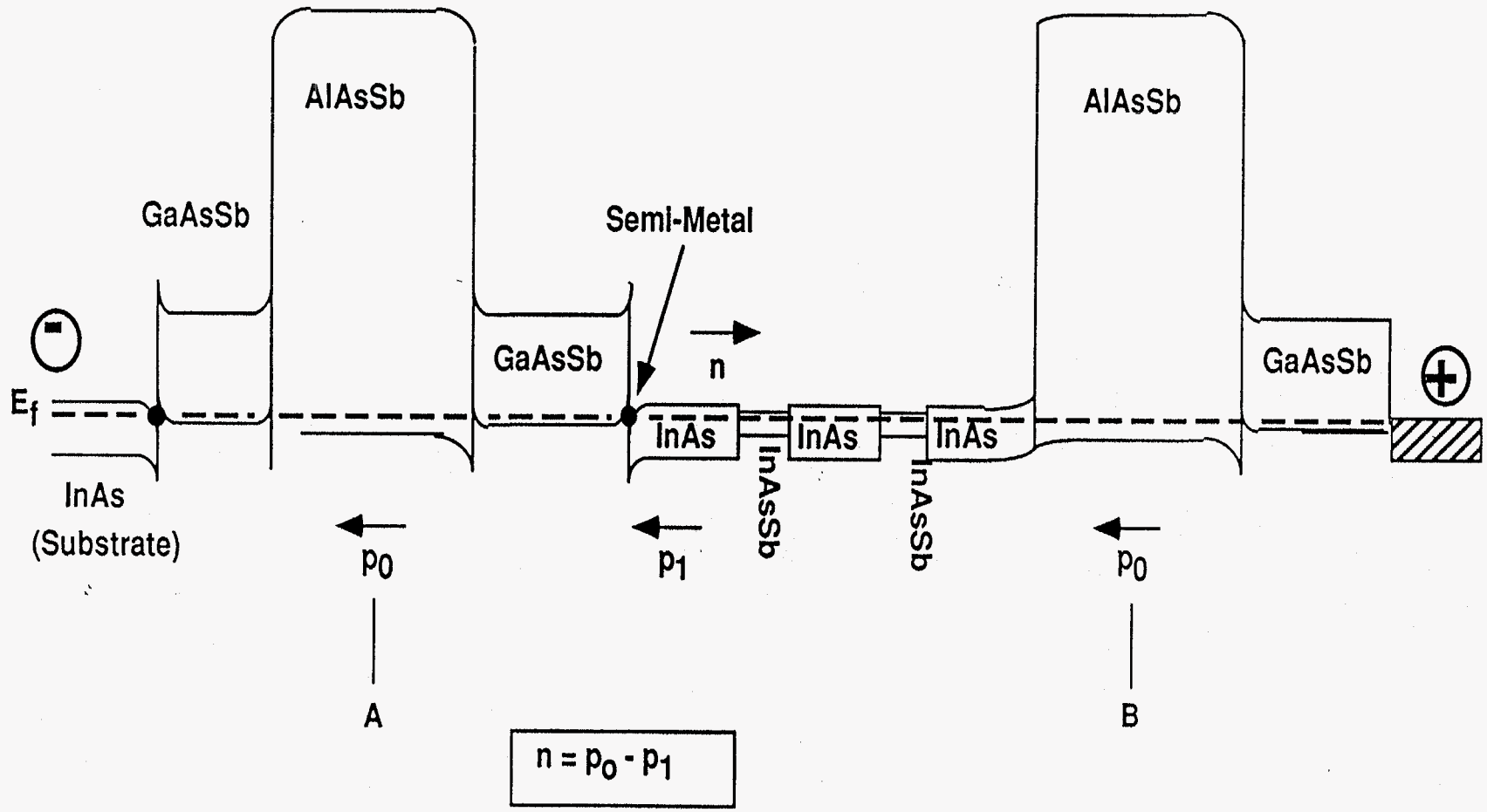
AlAsSb
GaAsSb
Semi-Metal
GaAsSb
n
AlAsSb
GaAsSb
E_f
InAs
(Substrate)
InAs
InAs
InAs
InAsSb
InAsSb
p0
p1
p0
A
B
n = p0 - p1

Figure 4.

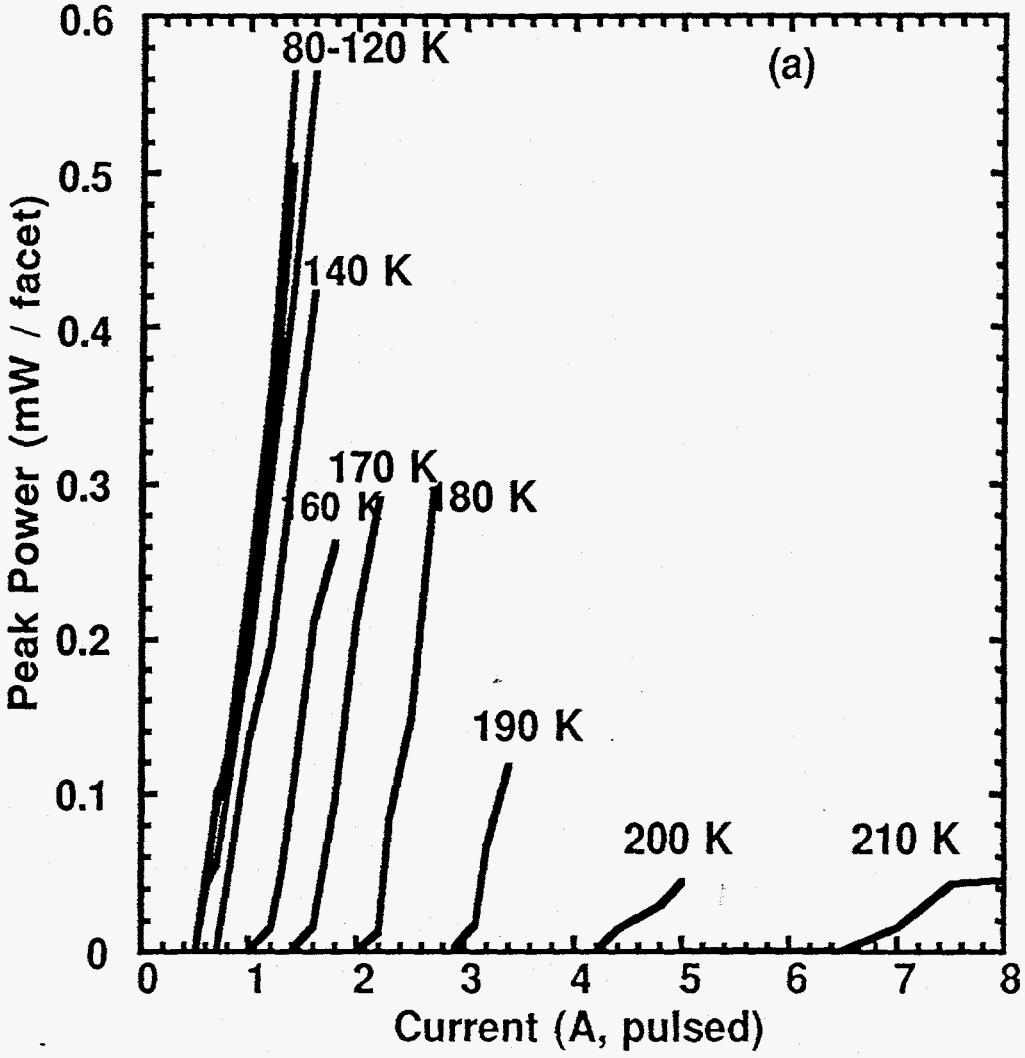
0.6
0.5
0.4
0.3
0.2
0.1
0
Peak Power (mW / facet)
80-120 K
(a)
140 K
170 K
60 K
180 K
190 K
200 K
210 K
0
1
2
3
4
5
6
7
8
Current (A, pulsed)

Figure 5a.

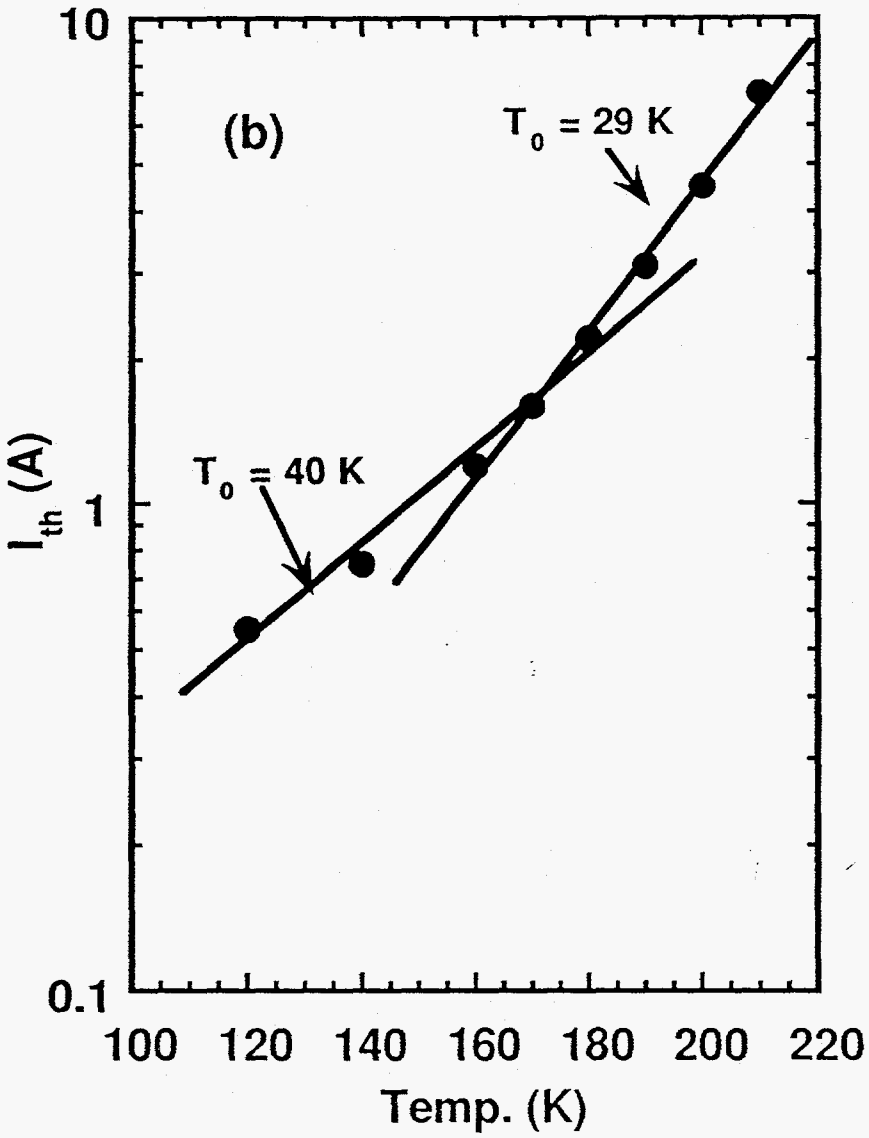


Figure 5b.

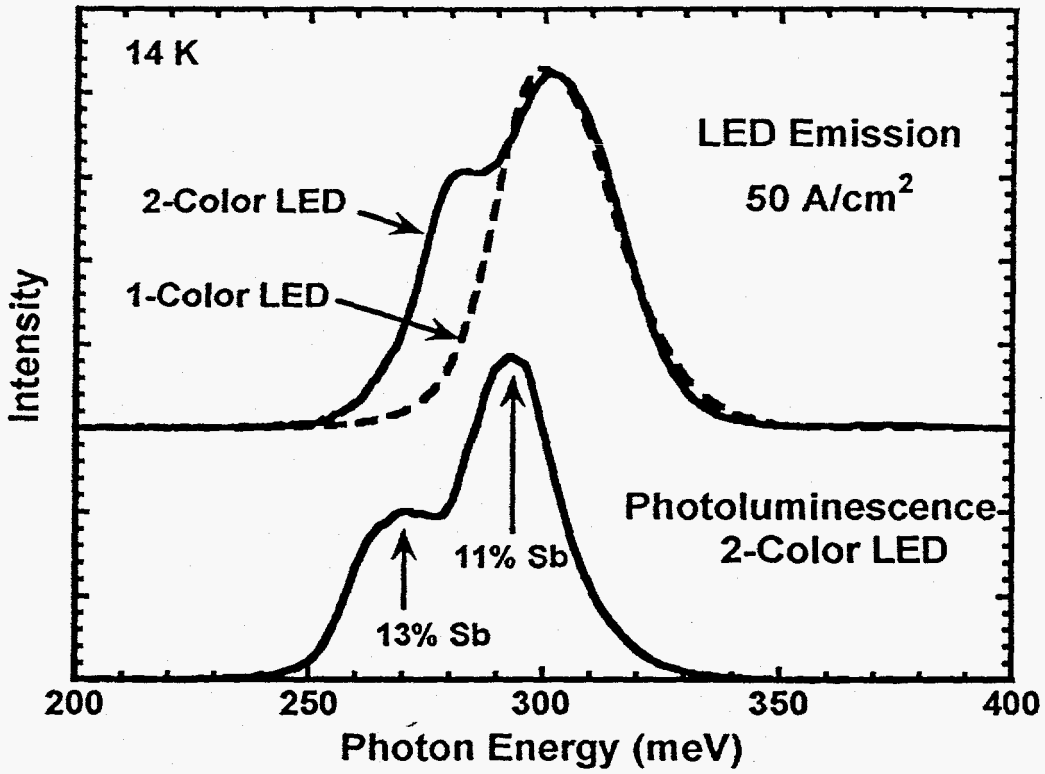
14 K
LED Emission
50 A/cm2
2-Color LED
1-Color LED
Intensity
Photoluminescence
2-Color LED
11% Sb
13% Sb
200
250
300
350
400
Photon Energy (meV)

Figure 6.

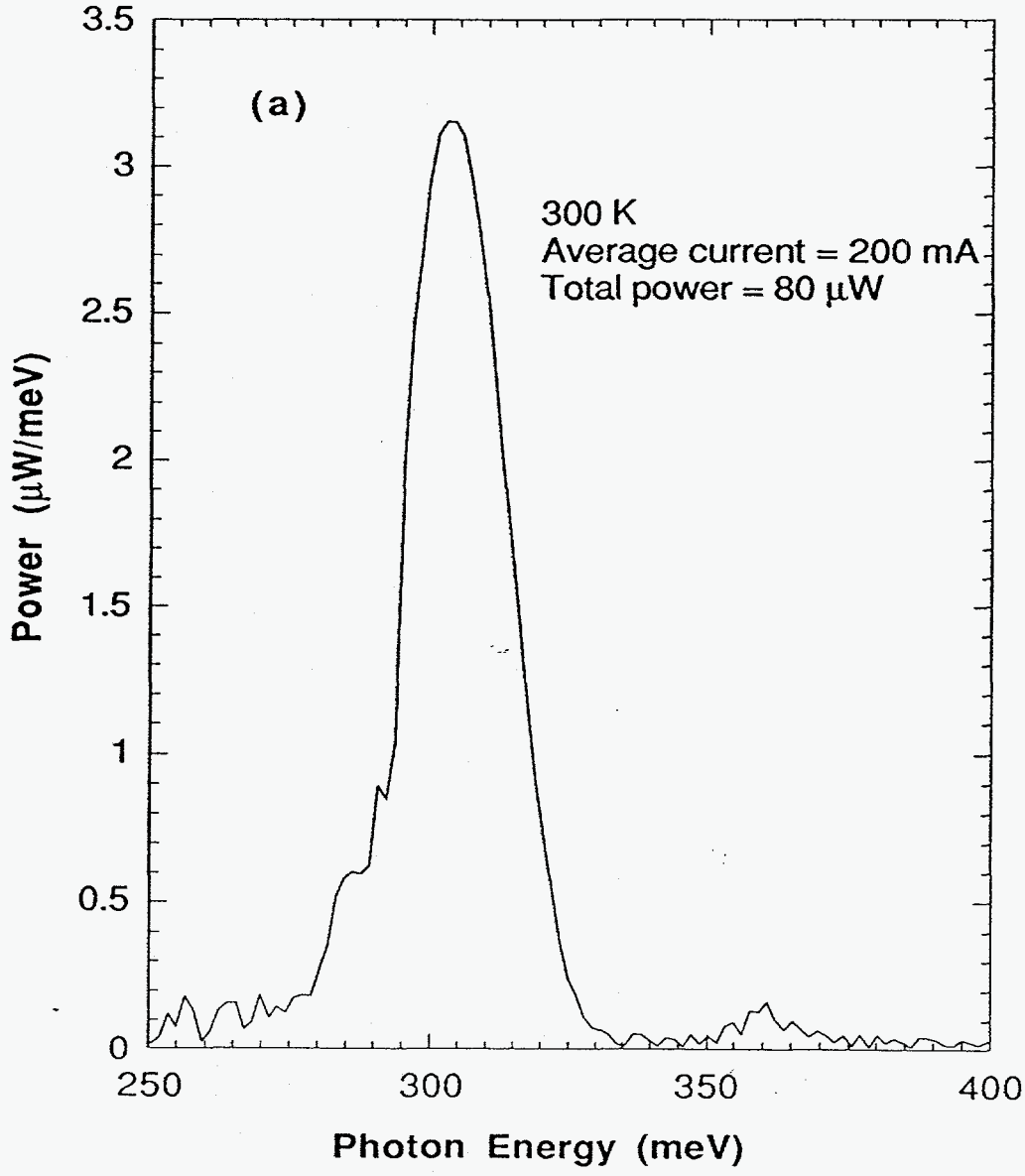
(a)
300 K
Average current = 200 mA
Total power = 80 μW
Power (μW/meV)
Photon Energy (meV)
3.5
3
2.5
2
1.5
1
0.5
0
250
300
350
400

Figure 7a.

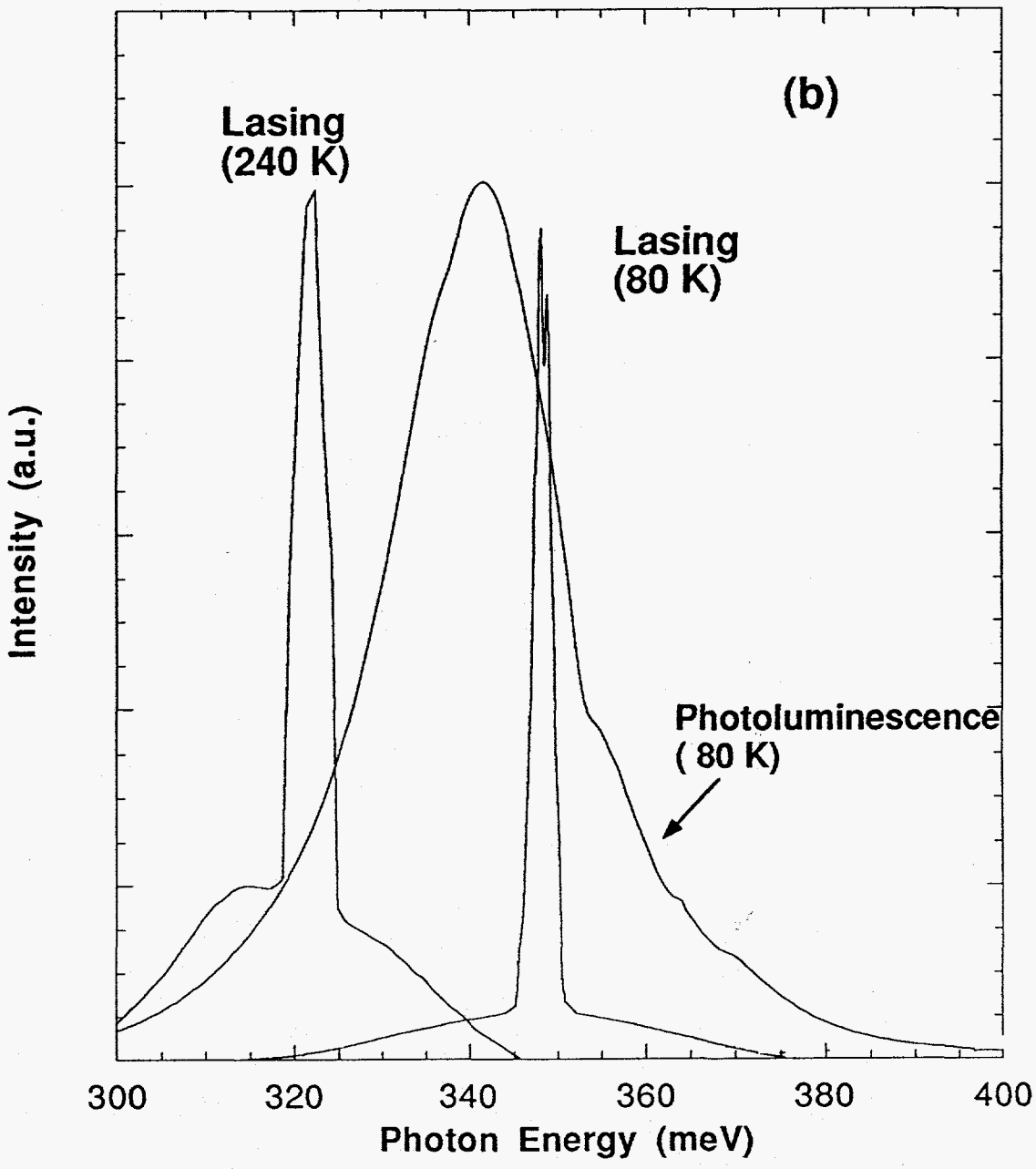
(b)
Lasing
(240 K)
Lasing
(80 K)
Photoluminescence
( 80 K)
Intensity (a.u.)
300
320
340
360
380
400
Photon Energy (meV)

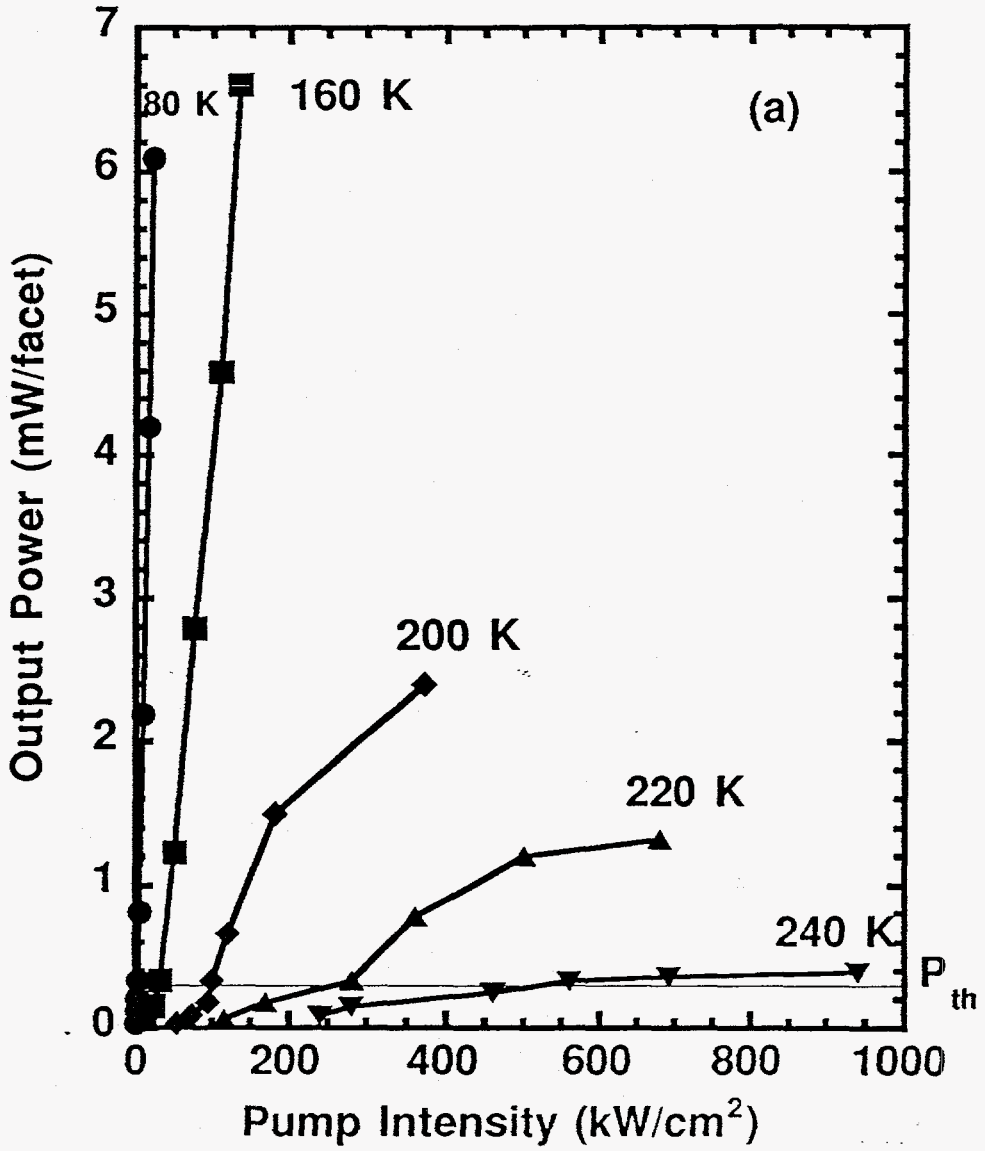
7
6
5
4
3
2
1
0
Output Power (mW/facet)
30 K
160 K
(a)
200 K
220 K
240 K
P th
0
200
400
600
800
1000
Pump Intensity (kW/cm2)

Figure 8a.

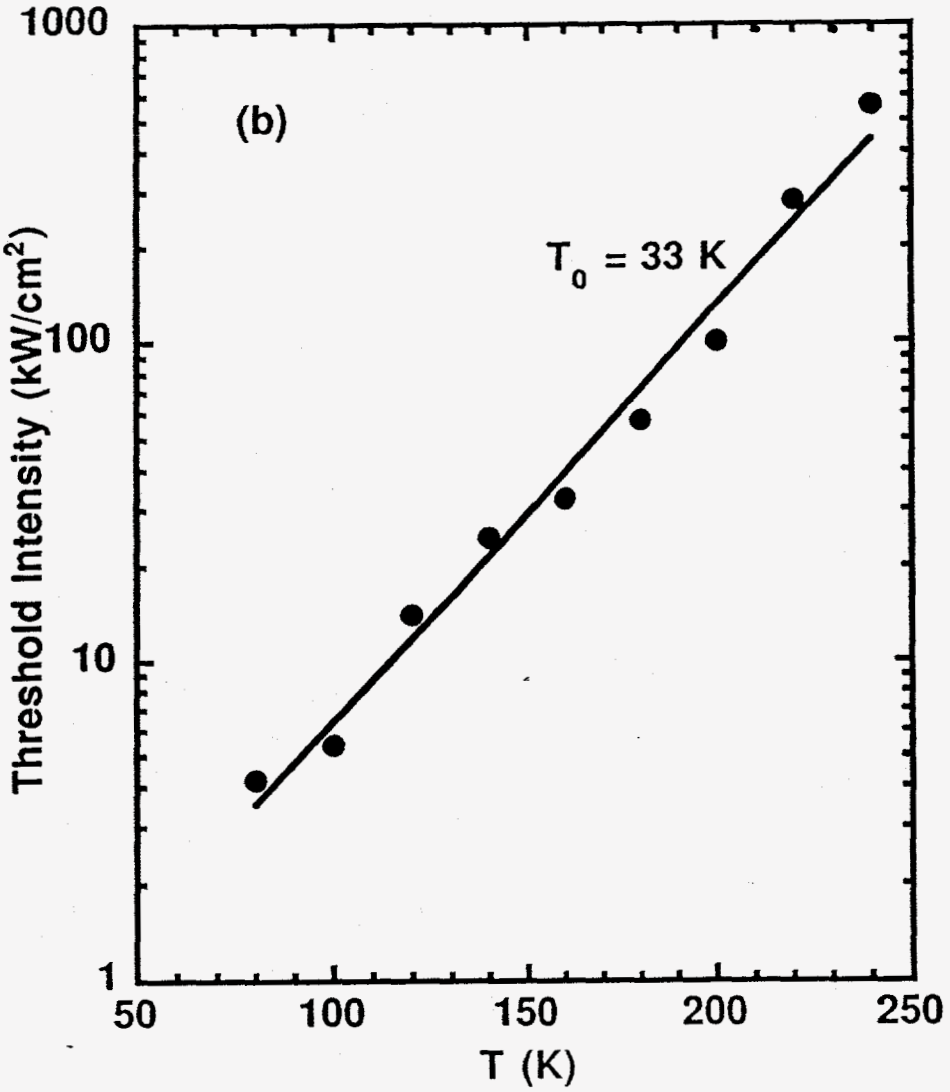
1000
100
10
1
(b)
$T_0$ = 33 K
Threshold Intensity (kW/cm$^2$)
50
100
150
200
250
T (K)

Figure 8b.